

Comparison and validation of three global-to-beam irradiance models against ground measurements

Pierre Ineichen

Center of Energy, University of Geneva, Battelle Bat A, 7 Rte de Drize, 1227 Carouge, GE, Switzerland

Received 28 March 2007; received in revised form 23 July 2007; accepted 13 December 2007

Available online 14 January 2008

Communicated by: Associate Editor David Renne

Abstract

The study presents a comparison and validation of 3 state of the art-global-to-beam irradiance conversion models against ground measurements from 22 sites covering a wide range of latitudes, altitudes and climates. One of the 3 models takes into account a climatic turbidity and gives slightly better results in terms of bias and precision.

On a hourly time step basis, the validation on over 100,000 station-hour values shows that the normal beam irradiance can be evaluated from the global horizontal component with a negligible bias and a precision of 85 W m^{-2} or 23%.

When the models are used on data with a shorter time step, the performance decreases, but remains acceptable. With a modification of the DirIndex (or the DirInt) model, the performance can slightly be increased and reach a bias of 2% and a precision of 28% for 10 min data.

© 2007 Elsevier Ltd. All rights reserved.

Keywords: Global and beam irradiance; Diffuse fraction; Model validation

1. Introduction

When dealing with solar irradiance in the field of architecture, solar engineering, and alternative summer cooling, the knowledge of irradiance time series is necessary to conduct buildings simulations, solar systems evaluations or solar plants design. If climatic databanks and real time series are relatively easy to find for specific locations and the global irradiance, it is not the case for the beam and diffuse, and these components are of great importance when converting the data into inclined impinging irradiance or specific components like for example daylight or PAR radiation.

The purpose of the present study is to do a comparison and a validation of the 3 state of the art-global-to-beam conversion models against measurements from 22 ground stations covering a wide range of climates, latitudes and altitudes. The Erbs model, an old and simple diffuse frac-

tion model which is still recommended in national standards, is also included as a reference for the performance assessment.

2. The models

2.1. Erbs model

The first correlation between the hourly clearness index K_t and the corresponding diffuse fraction was developed in 1977 by Orgill and Hollands and was based on 4 years data acquired in Toronto. The diffuse irradiance was measured with a shadowband pyranometer. In 1982 Erbs et al. adapted this correlation to extend it to latitudes from 31° to 42° North, and validated it on data from United States, based on pyrheliometric measurements. The correlation is divided into 3 zones: a linear regression for $0 < K_t \leq 0.22$, a fourth degree polynomial for $0.22 < K_t \leq 0.8$ and equal to a constant for $K_t > 0.8$.

E-mail address: pierre.ineichen@cuepe.unige.ch

2.2. DirInt model

The DirInt global to direct model (Perez et al., 1992) is based on a quasi-physical model, the DISC model, developed by Maxwell (1987), which has the form of a clear sky irradiance based on a Linke turbidity factor equal to 2.2, attenuated by a function of the clearness index K_t . This beam component is then corrected by a function of the modified clearness index K'_t as defined in Perez et al. (1990), the solar zenith angle, the atmospheric water vapor column and a stability index that accounts for the dynamics of the time series. The corresponding coefficients are obtained from a four-dimensional lookup table consisting of a $6 \times 6 \times 5 \times 7$ matrix.

2.3. DirIndex model

In the DirInt model described above, the four input parameters do not take into account the atmospheric turbidity, or only in a very slight manner with the clearness index K'_t . This comes from the fact that the atmospheric turbidity has a much higher influence on the beam irradiance than on the global component attenuation. The DirInt model was developed with a hypothesis of an average Linke turbidity factor of $T_L = 3$.

In the DirIndex model, the turbidity is taken into account by using DirInt in a relative mode (Perez et al., 2002). The model is used twice, once to calculate an intermediate beam irradiance G_{bn1} from the measurements of the global irradiance H_h , and a second time to calculate an intermediate clear sky beam irradiance G_{bn2} from H_{hc} ,

the modeled clear sky global irradiance. The formulation is the following:

$$G_{bn} = G_{bnc}(G_{bn1}/G_{bn2})$$

where G_{bnc} is the clear sky beam irradiance component. In the present study, the Solis clear sky model (Mueller et al., 2004; Ineichen, 2006) is used in its simplified version (Ineichen, 2008), it has the advantage to take into account the aerosol optical depth and water vapor content to evaluate both beam and global irradiance components.

2.4. Skartveit and Olseth model

Following the idea of Perez et al. (1992), Skartveit and Olseth modified their diffuse fraction model and introduced an hour-to-hour variability index (Skartveit et al., 1998). If the basic concept of the model is similar to the DirInt model and needs the same input parameters, the main difference is that its driving functions are analytical and continuous rather than based upon lookup tables as in the DirInt and DirIndex models.

The description is given in Skartveit et al. (1998).

3. Measurements

The data from 22 high quality ground stations were collected to conduct the validation. The sites cover latitudes from 8°N to 58°N, altitudes from sea level to 1600 m and a great variety of climates. Except for Lisboa and Lyon, where the beam irradiance is retrieved from diffuse measurements, the normal beam irradiance is available for all

Table 1
Ground sites used for the validation and comparison

	Station	Climate	Latitude	Longitude	Altitude	Notes
1	Albany NY (2001)	Humid continental	42.7	−73.9	100	ASRC – SUNYA
2	Albuquerque, NM (1999)	Arid	35.1	−106.7	1532	Sandia Natl. Labs, ARM protocol
3	Austin TX (2002)	Dry continental/subtropical	30.3	−97.8	180	University of Texas
4	Burlington KS (1999)	Dry continental	38.2	−95.6	358	ARM-SGP extended facility
5	Burns, OR (2002)	Semi-arid	43.6	−119.0	1265	Pacific Northwest network (SRML, 2003)
6	Carpentras (1999)	Mediterranean	44.1	5.1	100	BSRN – EPFZ
7	Desert Rock (2002)	Desert	36.6	−116.0	1000	SURFRAD network (2002)
8	Eugene, OR (2002)	Temperate maritim	44.1	−123.1	150	Pacific Northwest network
9	FSEC Cocoa, FL (1999)	Subtropical	28.3	−80.7	8	Florida Solar Energy center
10	Freiburg, D (1993–1994)	Temperate-humid	48.0	7.8	300	Frauenhofer Institute
11	Geneva, CH (1994–03)	Semi-continental	42.6	6.1	420	CUEPE – UNIGE
12	Gladstone, OR (2000)	Temperate humid	45.4	−122.6	98	Pacific Northwest network
13	Golden, CO (2000–2001)	Semi-arid	39.8	−105.2	1600	NREL
14	Hermiston, OR (1999–2000)	Temperate semi-arid	45.8	−119.4	180	Pacific Northwest network
15	Klamath Falls, OR (2000)	Temperate semi-arid	42.2	−121.7	1220	Pacific Northwest network
16	Kramer Junction, CA (1999)	Desert	35.0	−117.5	824	SEGS power plant monitoring
17	Kwajalein, Marshall Islands (2004)	Hot and humid maritime tropical climate	7.7	−167.7	8	BSRN – EPFZ
18	Lisboa, P (1994)	Temperate humid	38.8	−9.1	106	General class IDMP station
19	Lyon F (2004)	Moderate maritime/mediterranean	45.8	4.9	170	General class IDMP station
20	Payerne CH (2004)	Moderate maritime/continental	46.8	7.9	491	BSRN – EPFZ
21	Tamnanrasset, AL (2004)	Dry, desert	22.8	5.5	1400	BSRN – EPFZ
22	Toravere Estonia (2004)	Cold humid	58.3	26.5	70	BSRN – EPFZ

stations. High precision instruments (K + Z cm10, Eppley PSP and NIP) are used to acquire the data. A stringent calibration, characterization and quality control was applied on all the data by the person in charge of the measurements (following IDMP recommendations CIE (1994), BSRN (2002) network, ARM (2002), Pacific Northwest Network), the coherence of the data was verified by the author.

The list of the stations, their climate, latitude, longitude, and altitude are given in Table 1.

If the time step of the original data is below 60 min, they are averaged to bring them to hourly data. The total amount of hourly values is over 100,000.

For the station of Geneva and the year 2006, the model performance for sub-hourly time step is also investigated. The measurements are taken every 10 s, averaged and acquired on a minute basis. The values are then averaged to obtain 5, 10, 15, 30 and 60 min data.

4. Input parameters

The input parameters used in the present study, i.e. the atmospheric water vapor content and the aerosol optical depth, are retrieved from different climatic databases such as SODA (2002), Satel-Light (2002), Meteonorm (2003) or Randel et al. (1996). They are representative of average conditions and are mainly the results of interpolation between ground stations, sometimes with the help of satellite data. The databanks provide 12 monthly values for each location and each parameter. To avoid discontinuities between different months, the 12 values are smoothed over the year as illustrated in Fig. 1 for the Linke turbidity coefficient and the station of Hermiston.

For the south-west United States stations, the water vapor climatological data are retrieved from Randel et al.

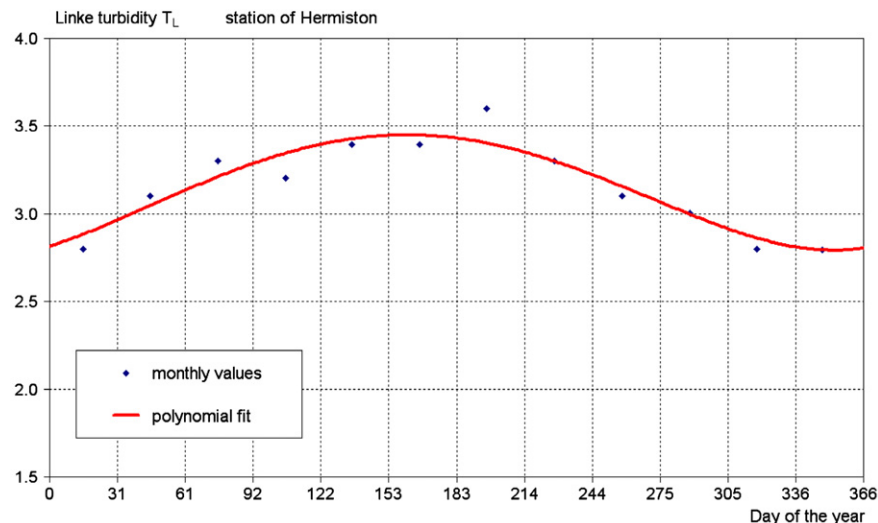


Fig. 1. Monthly average Linke turbidity values for the station of Hermiston with the corresponding smoothed line.

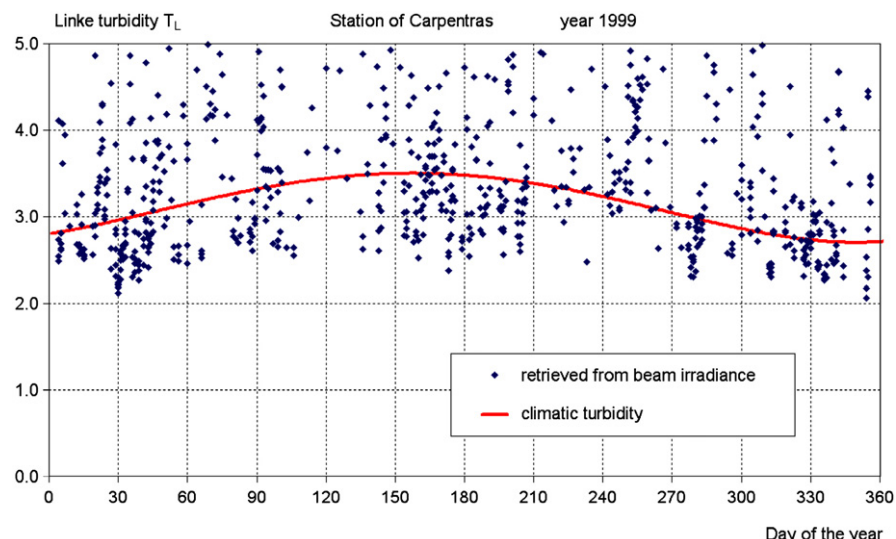


Fig. 2. Seasonal variation of the Linke turbidity. The values retrieved from the measurements are represented by blue dots, the climatic values by the red line. (For interpretation of the references to colour in this figure legend, the reader is referred to the web version of this article.)

(1996), for the other stations either from SODA (2002) or from Meteonorm (2003).

The turbidity has the highest influence on the atmospheric transmittance, but is also the most difficult to find, because it is not a synoptic parameter. In the present study, the Linke turbidity factor is used to parameterize the aerosol content of the atmosphere; it is not the best parameter, but it can be found in several climatic databanks such as SODA (2002). It is then converted to aerosol optical depth with the help of a model developed by Ineichen (2006) and given in the Appendix.

The majority of the measuring stations are situated in suburbs or city centers. As the use of urban type aerosols in the Solis model gives better results than rural type, only urban aerosols are considered in the present study.

It has to be noted that these climatic values are not representative of the clearest conditions. In Fig. 2, the Linke

turbidity factor T_L is retrieved from the normal beam irradiance with the help of the Kasten pyrheliometric formula applied on data corresponding to an air mass equal to two (Kasten, 1980). The lower limit of the dots corresponds to the clearest conditions. It can be seen here that the line, representative of the climatic smoothed values, retrieved from Soda is about one unit higher.

5. Comparison method

In terms of validation, when evaluating derived parameters with the same time step, the comparison is generally done hour by hour, by means of scatter plots, mean and absolute bias differences, and root mean square differences.

The scatter plot, or the representation of the modeled parameter versus the corresponding measured value is illus-

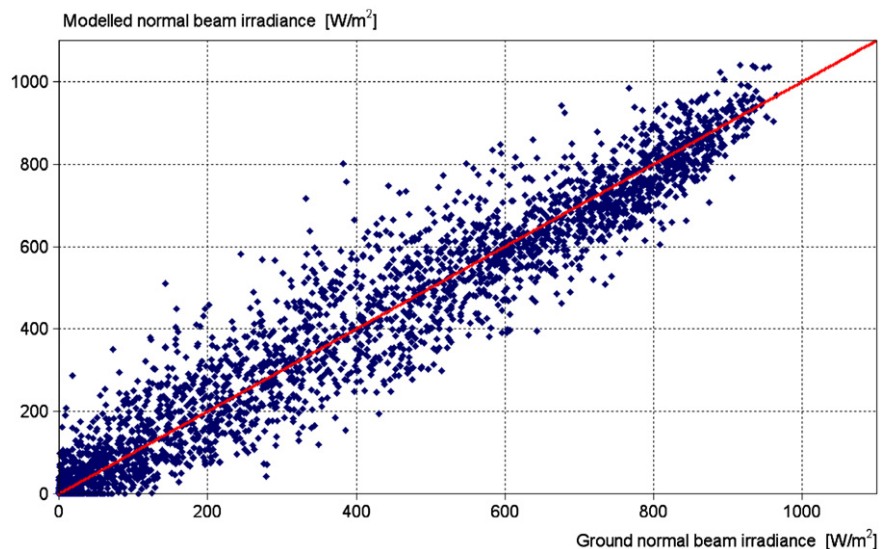


Fig. 3. Modeled versus ground normal beam irradiance scatter plot.

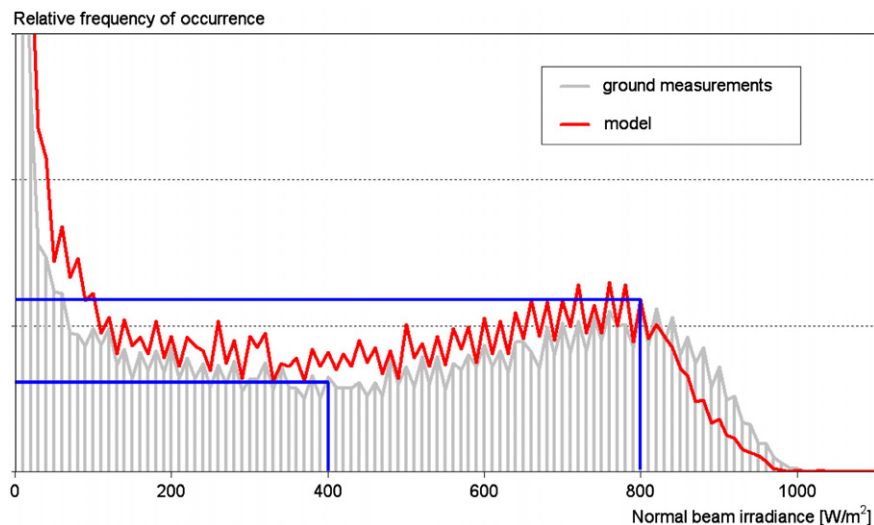


Fig. 4. Frequency of occurrence comparison. The ground measurements are represented by the grey bars, and the modeled values by the red line. (For interpretation of the references to colour in this figure legend, the reader is referred to the web version of this article.)

trated in Fig. 3. A perfect model should align the dots on the diagonal line.

The statistical parameters like the mean bias difference (mbd), the root mean square difference (rmsd) and the standard deviation or the dispersion around the bias (sd) represent a quantification of the model's precision. The mbd is expressed as the “model-measurements” difference, such as a positive bias represents a model overestimation.

In the field of architecture and natural light, the comparison is often done in terms of frequency of occurrence. In

this case, the graph is a line (or a bar chart) representative of the relative frequency of occurrence of a given parameter. This is illustrated in Fig. 4 for the normal beam irradiance. Here, for example, a value of 800 W m^{-2} occurs two times more than a value of 400 W m^{-2} .

6. Validation and comparison

The overall tendency of the scatter plots shows a good agreement between models and ground measurements as

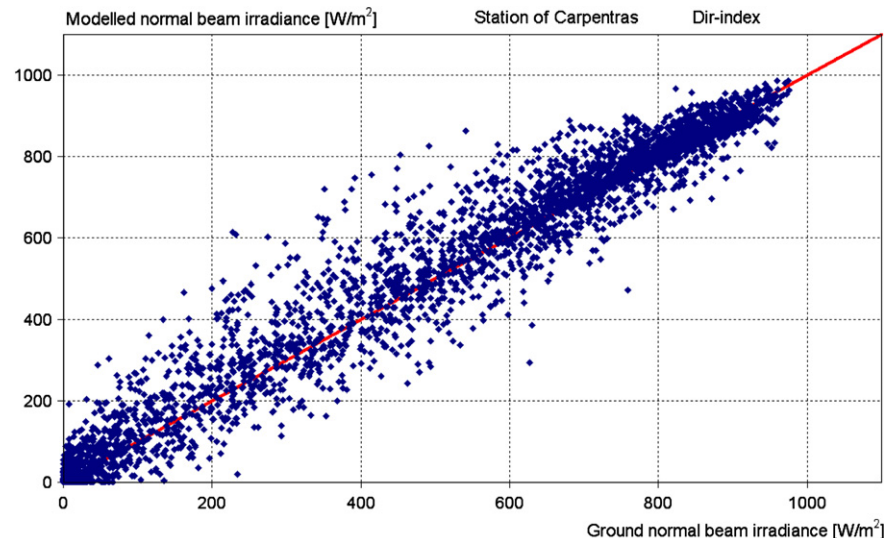


Fig. 5. Modeled versus ground normal beam irradiance scatter plot for the station of Carpentras and the DirIndex model.

Table 2

Mean bias difference, root mean square difference and standard deviation for all the stations and models

Station	nb	Average (W/m^2)	DirIndex			DirInt			Skartveit			Erbs		
			mbd	rmsd	sd	mbd	rmsd	sd	mbd	rmsd	sd	mbd	rmsd	sd
Albany	2604	381	10	85	84	-8	84	83	-17	83	81	-26	100	97
Albuquerque	3660	656	-8	96	96	-16	92	90	-34	110	105	-48	128	118
Austin	3504	359	22	96	93	-9	89	88	-12	97	96	0	101	101
Burlington	3538	411	-13	86	85	-34	84	77	-39	89	80	-59	125	110
Burns	3857	534	40	117	110	32	112	107	16	110	109	4	131	131
Carpentras	3969	386	17	68	66	17	68	66	2	68	68	-18	90	88
Cocoa	3570	378	3	108	108	-54	110	96	-55	114	100	-57	128	115
Desert Rock	3321	667	-14	112	1161	-141	109	109	-26	120	117	-27	116	113
Eugene	4026	385	-18	91	89	-15	83	81	-20	88	86	-43	124	116
Freiburg	3185	192	26	75	71	23	72	68	19	68	65	12	73	72
Geneva	37,282	265	0	68	68	-12	74	73	-16	72	70	-27	92	88
Gladstone	1250	307	-31	91	85	-29	89	84	-37	96	89	-53	115	102
Golden	7544	469	-5	103	102	-6	103	102	-15	107	104	-9	118	117
Hermiston	6715	454	-32	91	85	-23	85	82	-32	94	88	-46	114	103
Klamath	1869	501	-28	112	109	-39	109	501	-48	117	107	-68	142	125
Kramer	2644	733	-39	104	96	-43	101	92	-52	114	101	-67	121	101
Kwajalein	2714	362	60	122	106	8	95	95	6	94	94	14	99	98
Lisboa	1672	508	24	77	73	9	73	72	8	70	69	-3	90	89
Lyon	3758	294	-17	70	68	-25	77	73	-30	77	71	-37	91	83
Payerne	3990	286	31	84	78	28	83	79	19	82	80	11	84	83
Tamnrasset	3276	605	64	129	1102	12	123	100	65	128	110	28	125	122
Toravere	3604	234	6	73	73	15	75	74	6	72	71	2	88	88
all stations	105,562	370	-1	85	83	-10	85	82	-17	88	84	-26	105	99

The last line is the average over all stations except Kwajalein and Tamnrasset.

is illustrated in Fig. 5 for the station of Carpentras and the DirIndex model. The average mean bias difference is low (some %) and the precision of the 3 main models is around 87 W m^{-2} . The models taking into account the clearness index variability improve the precision of about 10–20% compared to the simple diffuse fraction Erbs model.

The complete statistics are given in Table 2, where the last line is the average over all stations except Kwajalein and Tamanrasset. If the mean biases vary around $\pm 40 \text{ W m}^{-2}$ and the precisions from 70 to 120 W m^{-2} , no particular pattern can be pointed out with latitude, altitude or climate. Also, if the precision is only very slightly better for the DirIndex model, the bias is negligible for the only model taking into account the atmospheric turbidity. This effect is visible for high values. It is illustrated for the station of Geneva in Figs. 6 and 7, where, respectively, the DirIndex and DirInt model scatter plots are represented.

The scatter plots for most of the analyzed stations are very similar to Geneva, except the stations of Klamath Falls, Kwajalein and Tamanrasset where patterns appear, probably due to instrumentation problems (cf. Appendix I).

The results are given in Charts I and II for all the stations and all the models. The bars on the right of the charts represent the average over all stations, except Kwajalein and Tamanrasset.

The previous statistics and plots show the overall performance of the models. The frequencies of occurrence show the specificity of each model. In Fig. 8, the DirIndex and the Skartveit model are represented. If for low normal beam values the two models show the same behaviour (overestimation), it is different for intermediate and high values. The Skartveit model gives better results for 600 – 800 W m^{-2} normal beam irradiances, but is not able to reproduce enough occurrences for values from 800 to 1000 W m^{-2} .

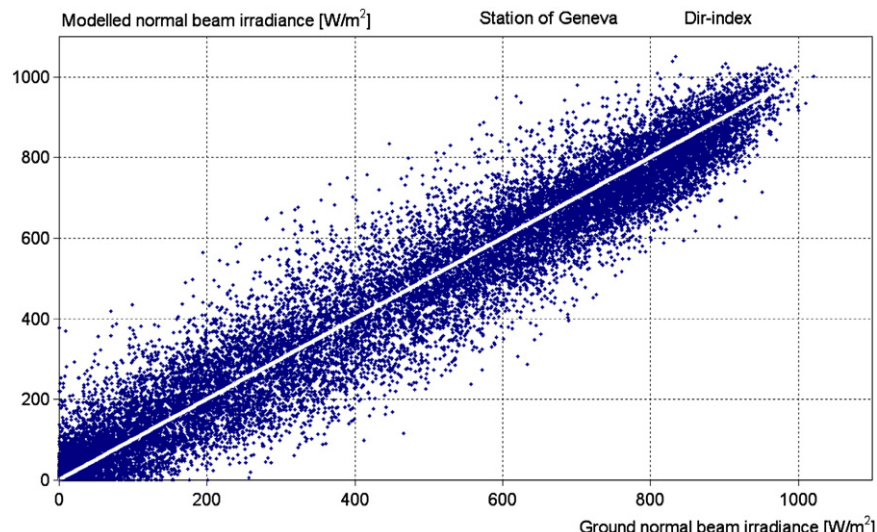


Fig. 6. Modeled versus ground normal beam irradiance scatter plot for the station of Geneva and the DirIndex model taking into account the turbidity.

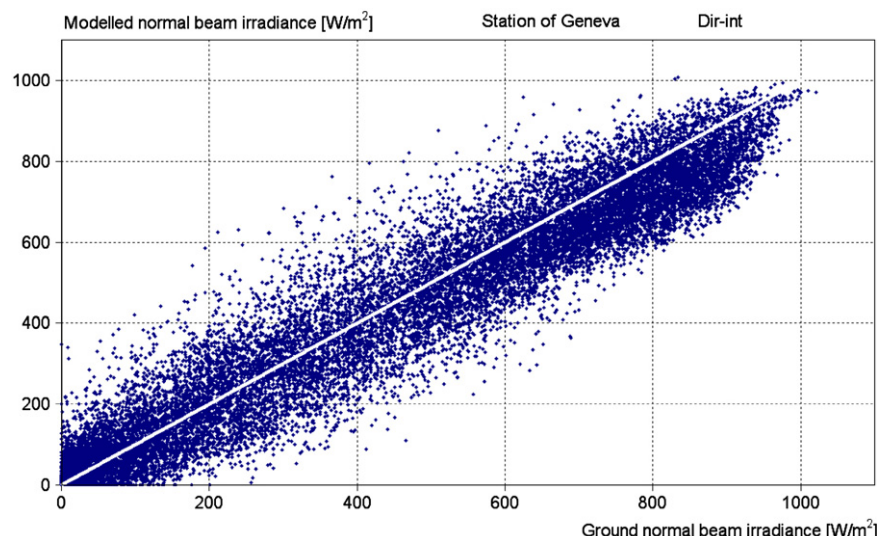


Fig. 7. Modeled versus ground normal beam irradiance scatter plot for the station of Geneva and the DirInt model.

In conclusion, the 3 state of the art-global-to-direct models have very similar behavior and are comparable in terms of bias and precision. Using water vapor and turbidity retrieved as monthly values from climatic databanks and the DirIndex model slightly improves the bias and the root mean square difference. As the turbidity can be very different from one day to the other, or even during a

day, a better knowledge of it could improve the precision of the produced beam irradiance.

7. Model performance for sub-hourly time step

The above comparison and validation is based on hourly data. This time step is widely used in most of the

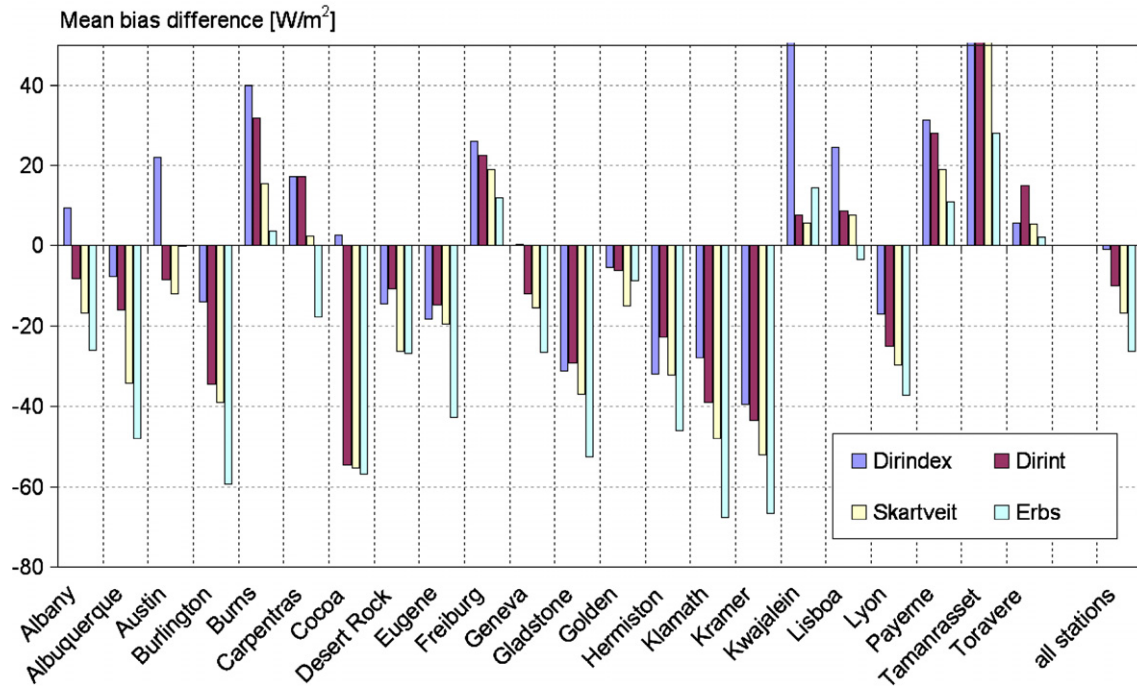


Chart I. Mean bias difference for all the stations and all the models. The “all stations” bars are the average except for Kwajalein and Tamanrasset.

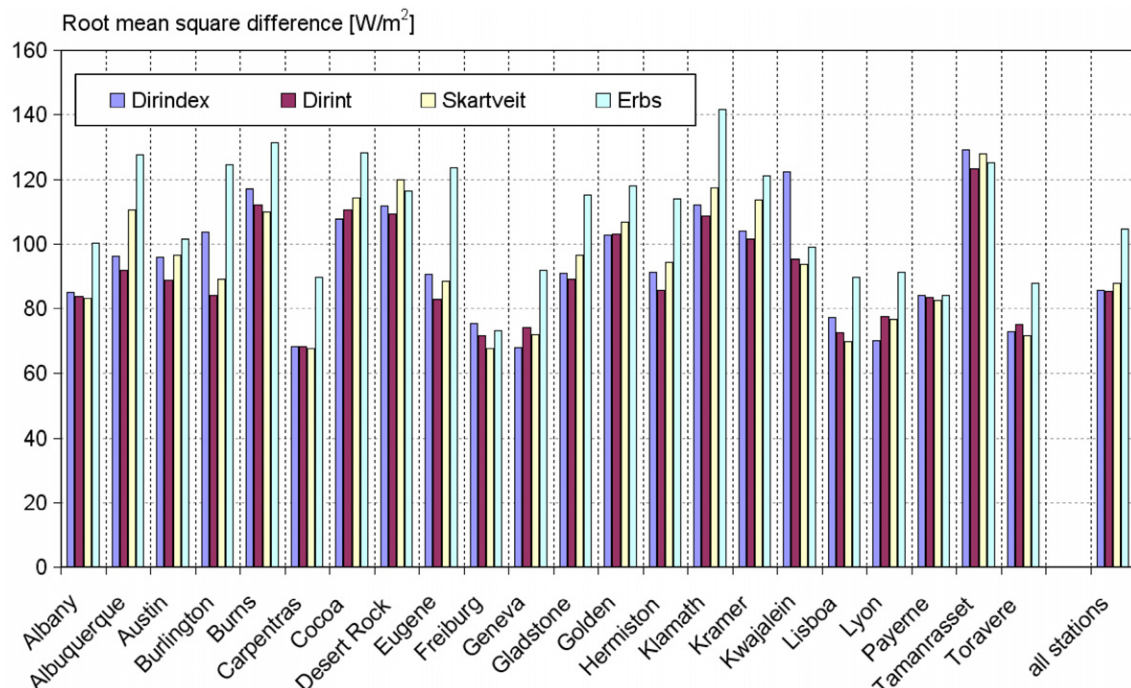


Chart II. Root mean square difference for all the stations and all the models. The “all stations” bars are the average except for Kwajalein and Tamanrasset.

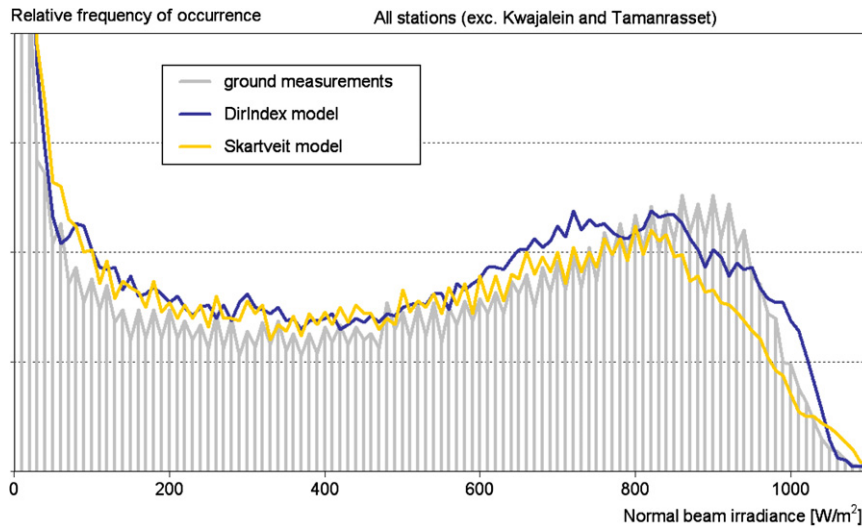


Fig. 8. Frequencies of occurrence comparison for the DirIndex and the Skartveit models.

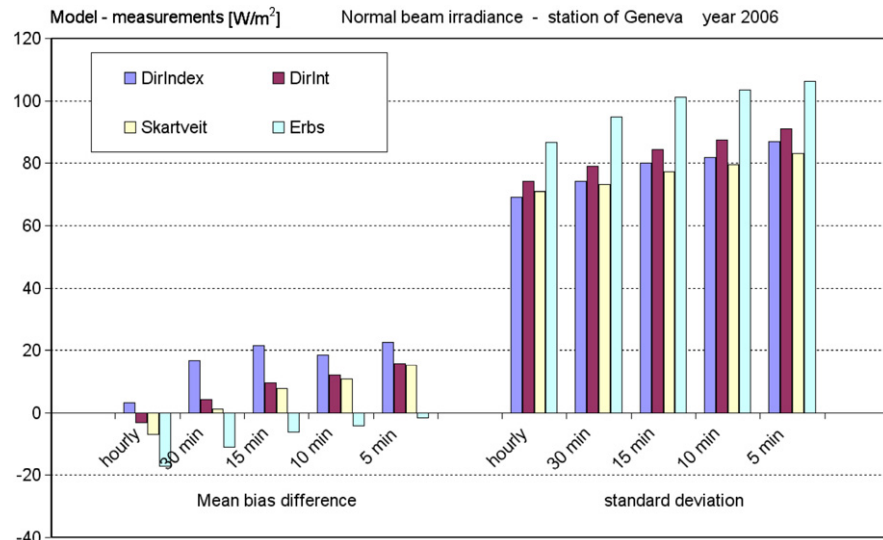


Chart III. Mean bias difference and standard deviation versus the integration period length for the DirIndex model.

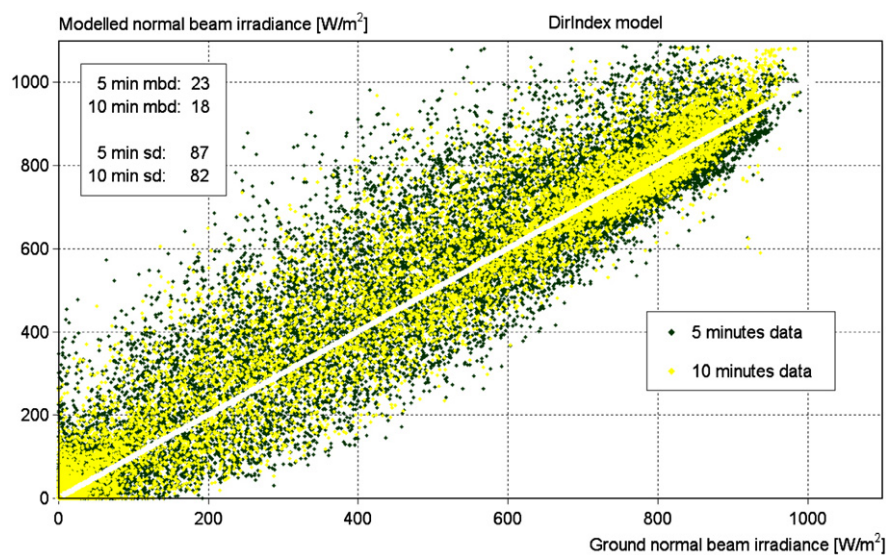


Fig. 9. DirIndex-modeled normal beam irradiance versus the corresponding measurements, for 5 and 10 min of integration period.

simulation processes. Since the launch of MSG (Meteosat Second Generation), the satellite images are now available every 15 min. As the satellite-derived beam irradiance is less effective than modeling the latter from satellite-derived global, it is interesting to investigate the applicability of the models on sub-hourly time step. This is done on data acquired in Geneva in 2006 and on time steps of 5, 10, 15, 30 and 60 min.

The first observation is that the overall dispersion increases with the decrease of the integration slot. Looking more into details, it appears that the dispersion increases more for intermediate conditions; this is a consequence of the integration period length: the increase of the integration period also increases the smoothing of the clearness index variability.

This is illustrated in [Chart III](#) where the mean bias difference and the standard deviation are represented for the five integration period lengths and the DirIndex model. The effect is comparable for the other models.

The comparison is done in [Figs. 9–11](#) where the scatter plots are given for 3 different integration period lengths. In these figures, the shorter integration period is plotted in dark dots and the longer period in clear dots. The effect of the integration period length on the dispersion is clearly visible. The results are given in [Table 3](#).

It is possible, by adding a multiplicative factor depending on the integration period length on the variability index, to slightly decrease the dispersion and the bias. The corresponding line in [Table 3](#) is labeled “10 min cor.”.

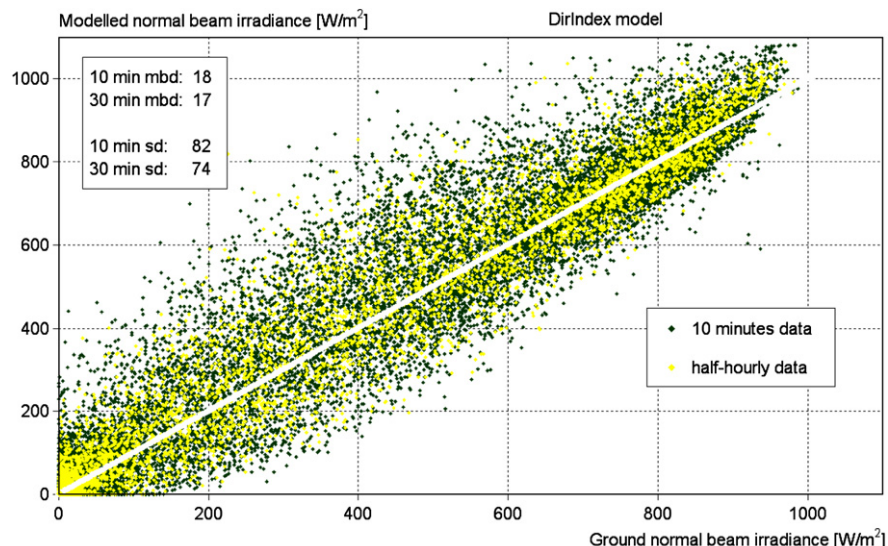


Fig. 10. DirIndex-modeled normal beam irradiance versus the corresponding measurements, for 10 and 30 min of integration period.

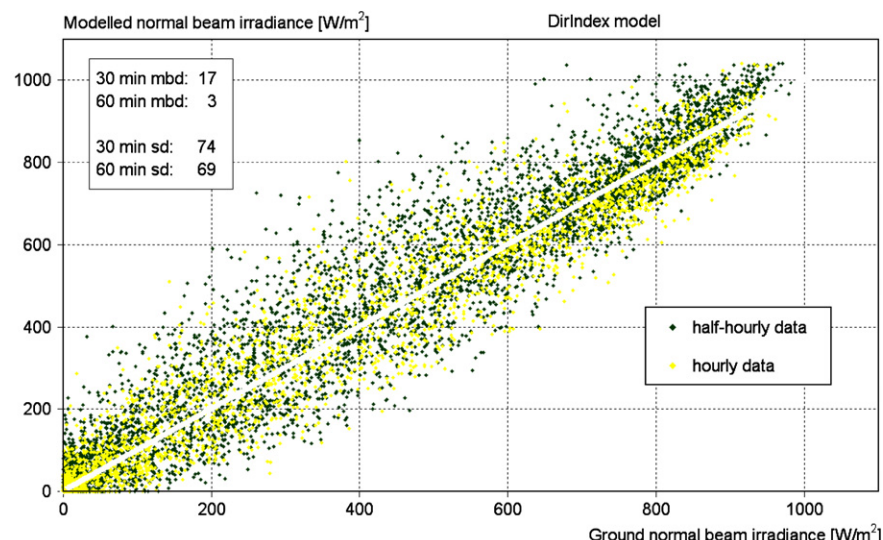


Fig. 11. DirIndex-modeled normal beam irradiance versus the corresponding measurements, for 30 and 60 min of integration period.

Table 3

Mean bias difference, root mean square difference and standard deviation for all the models and different time steps

Model	DirIndex			DirInt			Skartveit			Erbs		
	time step	nb	average	mbd	rmsd	sd	mbd	rmsd	sd	mbd	rmsd	sd
Hourly	3956	278	3	69	69	–3	74	74	–7	71	71	–17
30 min	7924	279	17	76	74	4	79	79	1	73	73	–11
15 min	15,772	279	22	83	80	9	85	84	8	78	77	–6
10 min cor.	23,679	279	6	79	79	0	83	83	–	–	–	–
10 min	23,679	279	18	84	82	12	88	87	11	80	80	–4
5 min	47,344	279	23	90	87	16	92	91	15	85	83	–2

In conclusion, the global-to-beam irradiance models can be used on data with a smaller time step without loosing too much in term of bias and precision. Nevertheless, the models were developed for hourly data and should be adapted for other integration period lengths.

8. Conclusions

Three global-to-beam irradiance models are validated against data from 22 ground stations covering a wide range of latitudes, altitudes and climates. The overall bias is very low and the precision is about $85\text{--}90\text{ W m}^{-2}$ or 23–24%, except for 2 sites where the results are slightly different and could be explained by either calibration problems or unadapted aerosol type.

The 3 models have very similar behavior and are comparable in terms of bias and precision. The use of the DirIndex model with water vapor and turbidity retrieved as monthly values from climatic databanks slightly improves the bias and the root mean square difference. A better knowledge of these parameters could improve the precision of the produced beam irradiance values.

All the models are developed on a hourly basis. The validation on data from Geneva with 5 different integration

time lengths shows that their performances decrease with the integration length, but remains acceptable.

Appendix I. Klamath Falls, Kwajalein and Tamanrasset stations analysis

For the station of Klamath and Tamanrasset, the patterns are similar for the different models; they are illustrated in Figs. A.1 and A.2, respectively. The common parameter between the 2 stations is the high altitude, but the patterns are opposite and cannot be found on the other 4 high altitude stations. As the patterns have the same tendency for all the models, and even if the acquisition stations are part of the BSRN network, a possible explanation could be instruments calibration or alignment problem. These results are excluded from the statistics because of the very high value of the mean bias difference.

For the station of Kwajalein, only the DirIndex model presents the highest bias and dispersion. The station is situated in the Marshall Islands, and the climate is hot, humid and tropical. In the clear sky model (Solis), urban type of aerosols is used for all the stations, and this is clearly not the case here and can explain the bad results with the DirIndex model. The two models using a constant average tur-

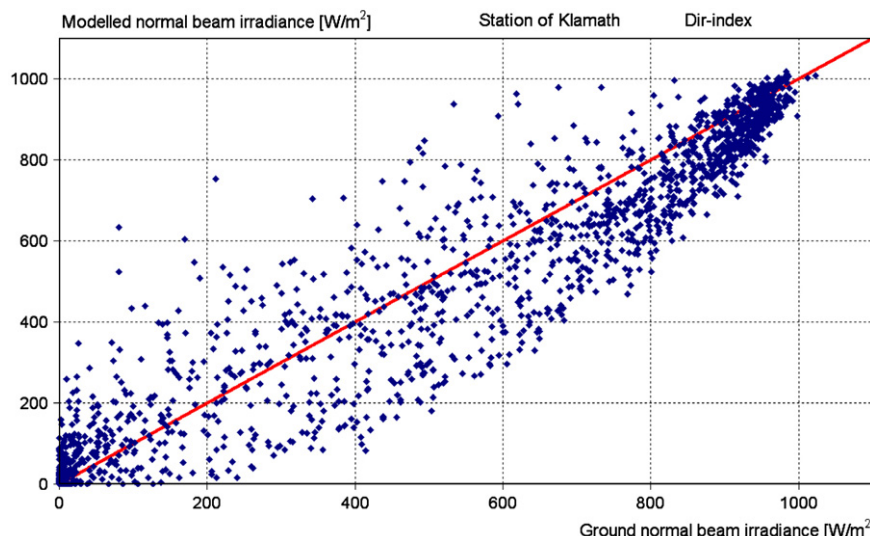


Fig. A.1. Modeled versus ground normal beam irradiance scatter plot for the station of Klamath and the DirIndex model.

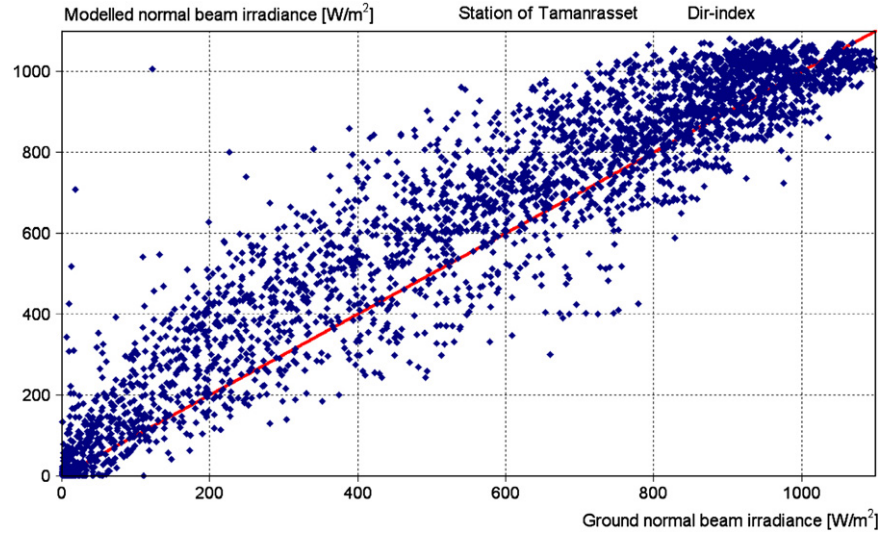


Fig. A.2. Modeled versus ground normal beam irradiance scatter plot for the station of Tamanrasset and the DirIndex model.

bidity present mean biases and precisions in the same range than all the other stations.

Appendix II. Conversion function between T_L and the aerosol optical depth

From numerically integrated spectral simulations done with Modtran (Berk et al., 1989), Molineaux et al. (1998) obtained the following expression for the broadband optical depth of a clean and dry atmosphere (fictitious atmosphere that comprises only the effects of Rayleigh scattering and absorption by the atmosphere gases other than the water vapor):

$$\Delta_{\text{cda}} = -0.101 + 0.235 * M^{-0.16}$$

and the broadband water vapor optical depth:

$$\Delta_w = 0.112 * M^{-0.55} * w^{0.34}$$

where w is the precipitable water vapor content of the atmosphere in (cm). The precision of these fits is better than 1% when compared with Modtran simulations in the range $1 < M < 6$ and $0 < w < 5$ cm. Using the Kasten pyrheliometric formula (1980), the Linke turbidity at $M = 2$ can then be written:

$$T_{L2}(\Delta_a, w) = -(9.4 + 0.9 * M) * \ln(\exp(-M * (\Delta_{\text{cda}} + \Delta_w + \Delta_a))) / M$$

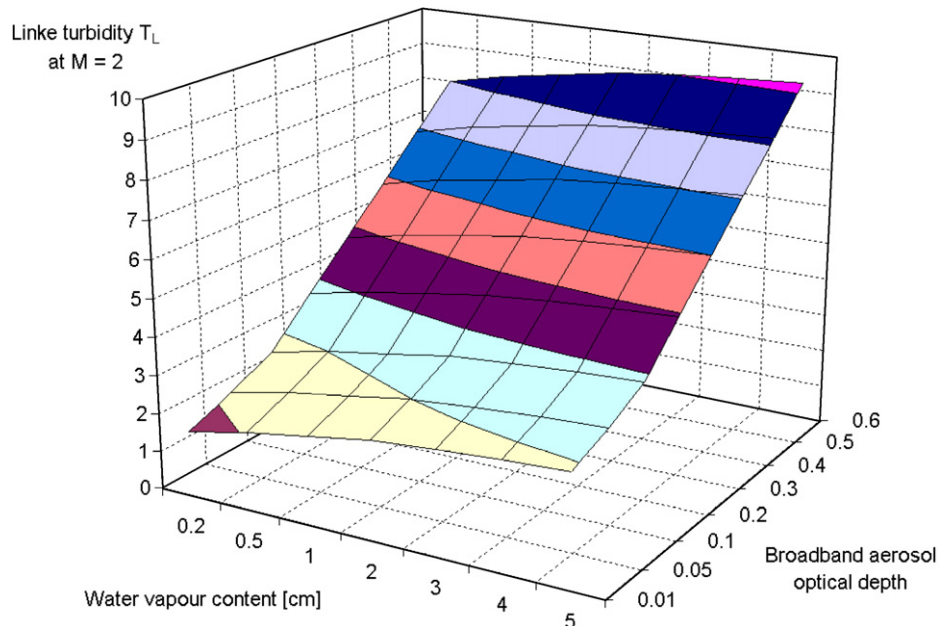


Fig. A.3. Linke turbidity T_L at airmass = 2 versus the aerosol optical depth and the atmospheric water vapor content.

with $\Delta_a = \delta_{a700}$ (Molineaux et al., 1998) or $\Delta_a = 0.27583*\delta_{a380} + 0.35*\delta_{a500}$ (Bird and Huldstrom, 1980).

This is illustrated in Fig. A.3. The inverse function can be used to convert the Linke turbidity T_L to the aerosol optical depth Δ_a . When dealing with other air masses than $M = 2$, the new formulation for the Linke turbidity defined by Ineichen and Perez (2002) should be used.

References

ARM, 2002. Atmospheric Radiation Measurement Program; <<http://www.arm.gov/>>.

BSRN, 2002. Baseline Surface Radiation Network, <<http://bsrn.ethz.ch/>>.

Berk, A., Bernstein, L.S., Robertson, D.C., 1989. MODTRAN: a Moderate Resolution Model for LOWTRAN 7. GL-TR-89-0122, updated and commercialized by Ontario Crp, 1996.

Bird, R.E., Huldstrom, R.L., 1980. Direct insolation models. *Trans. ASME J. Sol. Energy Eng.* 103, 182–192.

CIE, 1994. Guide to recommended practice of daylight measurements, CIE 108, ISBN 3 900 734 50x.

Erb, D.G., Klein, S.A., Duffie, J.A., 1982. Estimation of the diffuse radiation fraction for hourly, daily and monthly-average global radiation. *Sol. Energy* 28 (4), 293–304.

Ineichen, P., Perez, R., 2002. A new airmass independent formulation for the linke turbidity coefficient. *Sol. Energy* 73 (3), 151–157.

Ineichen, P., 2006. Comparison of eight clear sky broadband models against 16 independent data banks. *Sol. Energy* 80, 468–478.

Ineichen, P., 2008. A broadband simplified version of the solis clear sky model. *Sol. Energy* (accepted for publication).

Kasten, F., 1980. A simple parameterization of two pyrheliometric formulae for determining the Linke turbidity factor. *Meteor. Rdsch.* 33, 124–127.

Maxwell, E.L., 1987. A quasi-physical model for converting hourly global horizontal to direct normal insolation. Report SERI/TR-215-3087, Solar Energy Research Institute, Golden CO.

Meteonorm, 2003. <<http://www.meteotest.ch>>.

Molineaux, B., Ineichen, P., O’Neil, N., 1998. Equivalence of pyrheliometric and monochromatic aerosol optical depths at a single key wavelength. *Appl. Optics* 37 (30), 7008–7018.

Mueller, R.W., Dagestad, K.F., Ineichen, P., Schroedter-Homscheidt, M., Cros, S., Dumortier, D., Kuhlemann, R., Olseth, J.A., Piernavieja, G., Reise, C., Wald, L., Heinemann, D., 2004. Rethinking satellite based solar irradiance modelling – the SOLIS clear-sky module. *Remote Sensing Environ. Remote Sens. Environ.* 91, 160–174.

Orgill, J.F., Hollands, K.G., 1977. Correlation equation for hourly diffuse radiation fraction on a horizontal surface. *Sol. Energy* 19 (4), 357–359.

Perez, R., Seals, R., Zelenka, A., Ineichen, P., 1990. Climatic evaluation of models that predict hourly direct irradiance from hourly global irradiance: prospects for performance improvements. *Sol. Energy* 44 (2), 99–108.

Perez, R., Ineichen, P., Maxwell, E., Seals, R., Zelenka, A., 1992. Dynamic global to direct irradiance conversion models. *ASHRAE Trans. Res. Series*, 354–369.

Perez, R., Ineichen, P., Moore, K., Kmiecik, M., Chain, C., George, R., Vignola, F., 2002. A new operational model for satellite derived irradiances: description and validation. *Sol. Energy* 73 (5), 307–317.

Randel, D.L., VonderHaar, T.H., Ringerud, M.A., Stephens, G.L., Greenwald, T.J., Combs, C.L., 1996. A new global water vapor dataset. *Bull. AMS (BAMS)* 77 (6).

Satell-Light, 2002. The European database of daylight and solar RADIATION. <<http://www.satellight.com>>.

Skartveit, A., Olseth, J.A., Tuft, M.E., 1998. An hourly diffuse fraction model with correction for variability and surface albedo. *Sol. Energy* 63 (3), 173–183.

SODA, 2002. Integration and exploitation of networked solar radiation databases for environment monitoring. <<http://www.soda-is.com>>.

Solar Radiation Monitoring Laboratory, 2003. Department of Physics, 1274 University of Oregon. <<http://solardata.uoregon.edu/>>.

SURFRAD network – monitoring surface radiation in the continental United States (2002). NOAA, Surface Radiation Research Branch (<<http://www.srrb.noaa.gov/surfrad/index.html>>).